Aerotecnica Missili & Spazio, *The Journal of Aerospace Science, Technology and Systems*

Optimization of low-thrust trajectory for a mission to the asteroid 433 Eros with Earth gravity assist

N. Marmo[a]

[a] "Sapienza" - Università di Roma
Dipartimento di Ingegneria Meccanica e Aerospaziale
nicola.marmo.1@gmail.com

Abstract

Subject of this paper is the design of a space robotic mission to the asteroid 433 Eros. The mission aims to grab a boulder from its surface and transport it inside the Earth's Hill sphere. This kind of mission was chosen to develop a method of analysis of all the opportune trajectories for a sample-return mission, using a generic Near-Earth asteroid as 433 Eros. This work was inspired by NASA's Asteroid Redirect Mission, which was cancelled in 2017 due to lack of funding, and whose purpose was to transfer a boulder from the surface of a Near-Earth asteroid to a stable lunar orbit, where it could be further analysed both by robotic probes and by a future manned mission. The propulsion system used for the theorized mission consists of three autonomous ion thrusters fully adjustable in magnitude and direction of thrust. Furthermore, during the return flight an Earth gravity assist is used to increase the mass of boulder that the spacecraft can transport towards Earth. Selecting the same time window of the ARM, different trajectories, separately for the outbound and inbound flights, are calculated using indirect methods. Subsequently, a plausible interpretation of the different performances of the calculated trajectories is given, considering both the solar electric power available to the spacecraft and the geometric configuration of the bodies involved. At the end of this process, all the calculated trajectories for the outbound and inbound flights are compared, and possible final solutions for the mission are discussed.

1. Introduction

The optimization of an interplanetary trajectory is essential to satisfy all the scientific and technical requirements of a space mission. In particular, an optimal trajectory is defined by evaluating a control law for the spacecraft which is able to maximize a specified performance index, while fulfilling the boundary conditions that characterize the mission. Numerical methods for trajectory optimization can be in general classified into three main groups: indirect methods, direct methods, and evolutionary algorithms. This paper is focused in particular on the first group and on a specific application for a sample-return mission to an asteroid.

Indirect methods, as will be discussed in Paragraph 3, are based on the theory of optimal control and solve the optimization problem [1] by defining and solving a boundary value problem [2]. The theory of optimal control provides differential equations for the adjoint variables and boundary conditions for optimality. The optimal controls must maximize the Hamiltonian at any given point along the trajectory, in agreement with Pontryagin's Maximum Principle (PMP).

Indirect methods are some of the most efficient optimization methods for trajectory design of articulate interplanetary missions such as the asteroid missions. In fact, in these kind of missions, because low-thrust engines are normally chosen as propulsion systems, planetary fly-bys are often used as gravity assist either for the outbound or the inbound flight. Several space missions have been accomplished so far involving asteroid rendezvous and explorations. The first mission with an asteroid fly-by was the NASA mission Galileo which, during the observation campaign of the Jovian system, achieved an asteroid 951 Gaspra fly-by [3] and discovered the first asteroid moon, Dactyl, around asteroid 243 Ida in 1991 [4]. 951 Gaspra and 243 Ida are both asteroids of the main belt. The first asteroids visited instead by an ESA probe are 2867 Šteins and 21 Lutetia, two asteroids of the main belt, which have been observed by the spacecraft Rosetta during its journey to the comet 67P/Chutyumov-Gerasimenko, respectively in 2008 and 2010 [5, 8]. The JAXA mission Hayabusa, ended in 2010, is the first sample-return mission from an asteroid. The asteroid chosen for this mission was a small Near-Earth asteroid (NEA) named 25143 Itokawa. Another sample-return mission is the underway NASA mission OSIRIS-REx, whose goal is to study asteroid 101955 Bennu, a carbonaceous NEA in the Apollo group, and return a sample to Earth

in 2023. Both these two latter missions aimed to return samples which are used exclusively for chemical analysis and, for this reason, samples of a few grams are enough for this purpose. The NASA's Asteroid Redirect Mission (ARM) [7, 8] is instead a theorized sample-return mission which aims to grab a boulder from the surface of an asteroid and to place it on a stable lunar orbit for future analysis of robotic probes and manned missions. An experiment of "gravity tractor" was also planned for the ARM [9, 10] using the collected boulder. This method consists of making the mass of the spacecraft (18 tons [11]) and its boulder cargo (which should weights several tons) impart a gravitational force on the asteroid, slowly altering the asteroid's trajectory. In this way, the asteroid redirect vehicle would demonstrate the "gravity tractor" planetary defence technique on a hazardous-size asteroid. However, the ARM has been cancelled due to lack of funding.

Using indirect methods, an analysis and validation of the NASA's Asteroid Redirect Mission is conducted selecting a NEA. Besides defining the optimal trajectory for this mission by means of indirect methods, the main aim of this paper is to present a specific analysis on the optimal use of multiple thrusters in a context of sample-return mission from a NEA. Similar works about the trajectory design of the ARM are presented in the paper of R. G. Merrill, M. Qu et al. [12], while a generic study to investigate the feasibility of identifying, capturing, and returning an entire NEA is presented in the paper of D. Landau, J. Dankanich et al. [13]. Another feasibility study of a similar mission have been done in the paper of J. R. Brophy, R. Gershman et al. [14]. However, this latter paper investigate briefly all the different aspects of the mission, while the presented paper is focused on a preliminary analysis of the spacecraft trajectory considering the substantial mass increase of the spacecraft due to the collected boulder.

The optimization problem for this mission consists of finding the optimal power partitioning among the thrusters, the corresponding thrust magnitude and the optimal thrust direction. Typical assumptions for a preliminary analysis of the mission are made; more in detail, the patched-conic approximation is adopted and two-body problem equations are used to describe the interplanetary flight. Furthermore, cubic relations are assumed for thrust and propellant flow rate as a function of input power, since each engine can either be turned off or operate between minimum and maximum input power limits. In addition, the total power cannot exceed the available power, which varies inversely with the distance from the Sun.

The asteroid (433) Eros in chosen as target in order to provide a wide variation in power available for thrusting, as opposed to primary ARM asteroids with more Earth-like orbits [15]. Orbital elements of 433 Eros at the epoch JD 2458000.5 (4 September 2017) are reported in Table 1.

Table 1
Orbital elements of 433 Eros at the epoch JD 2458000.5 [16]

Aphelion	1.7825 AU
Perihelion	1.1334 AU
Semi-major axis	1.4579 AU
Eccentricity	0.2226
Orbital period	1.76 years
Mean anomaly	71.280°
Inclination	10.828°
Longitude of ascending node	304.32°
Argument of perihelion	178.82°

An Earth gravity assist in the return leg (modelled as an instantaneous rotation of the hyperbolic excess velocity at Earth encounter) is used to improve performance. In order to simplify the optimization process, a different analysis is carried out separately for the outbound and inbound flights: for the outbound flight the aim is to minimize the propellant consumption with a fixed initial mass of propellant and dry mass, while, for the inbound flight, the performance index to be maximized is the initial mass (i.e. the total mass of the spacecraft departing from the asteroid, so the mass of grabbed boulder) using, however, a proper fixed mass of propellant for the journey. After having combined two different legs among all the found assorted trajectories, a second optimization of the inbound flight is done using the real amount of propellant left from the selected outbound flight. In this fashion is possible to provide the mission with a complete trajectory.

2. Statement of the problem

In preliminary analysis, the patched-conic approximation is commonly adopted and the two-body problem equations are used to describe the motion of the point-mass spacecraft (with variable mass m). For the presented case, only the heliocentric phases are considered and the state equations are the following:

$$\frac{d\boldsymbol{r}}{dt} = \boldsymbol{v} \tag{1}$$

$$\frac{d\boldsymbol{v}}{dt} = \boldsymbol{g} + \boldsymbol{T}/m \tag{2}$$

$$\frac{dm}{dt} = -q \tag{3}$$

where r is the position vector and $\boldsymbol{v}$ the velocity vector. The value of the spacecraft initial mass is assigned and it is equal to 10000 Kg, of which 5000 Kg is the mass

of the available propellant. Escape and arrival velocity at the Earth's Hill sphere are both fixed at 1.4 Km/s (C3 equals to 1.96 $\mathrm{Km}^2/\mathrm{s}^2$). These previous values are chosen on the base of performance of the current technology. Boundary conditions can be written as:

$$\boldsymbol{r}_0 = \boldsymbol{r}_E(t_0) \tag{4}$$
$$[\boldsymbol{v}_0 - \boldsymbol{v}_E(t_0)]^2 = \mathrm{C3}_0 \tag{5}$$
$$m_0 = 10000 \text{ Kg} \tag{6}$$
$$\boldsymbol{r}_1 = \boldsymbol{r}_A(t_1) \tag{7}$$
$$\boldsymbol{v}_1 = \boldsymbol{v}_A(t_1) \tag{8}$$
$$\boldsymbol{r}_2 = \boldsymbol{r}_A(t_2) \tag{9}$$
$$\boldsymbol{v}_2 = \boldsymbol{v}_A(t_2) \tag{10}$$
$$m_2 - m_1 = m_{boulder} \tag{11}$$
$$\boldsymbol{r}_{3-} = \boldsymbol{r}_{3+} = \boldsymbol{r}_E(t_3) \tag{12}$$
$$[\boldsymbol{v}_{3-} - \boldsymbol{v}_E(t_3)]^2 = [\boldsymbol{v}_{3+} - \boldsymbol{v}_E(t_3)]^2 \tag{13}$$
$$\boldsymbol{r}_f = \boldsymbol{r}_E(t_f) \tag{14}$$
$$[\boldsymbol{v}_f - \boldsymbol{v}_E(t_f)]^2 = \mathrm{C3}_f \tag{15}$$
$$m_f = 5000 \text{ Kg} \tag{16}$$

where subscripts 0, 1, 2, 3 and f refer to Earth departure, Eros arrival, Eros departure, Earth gravity assist ($-$ just before, $+$ just after) and Earth arrival, respectively. Subscripts E and A refer to Earth and target asteroid.

Thrust magnitude and propellant mass flow rate of a thruster are related to its input power. As a consequence, the effective exhaust velocity (therefore the specific impulse) is also a function of the input power. Cubic relations are assumed here for thrust magnitude T and propellant mass flow rate q:

$$T = a_0 + a_1 P + a_2 P^2 + a_3 P^3 \tag{17}$$
$$q = b_0 + b_1 P + b_2 P^2 + b_3 P^3 \tag{18}$$

and the specific relationships applied in the example problems for this work are shown in Figure 1 (a). Additionally, the engine specific impulse as a function of input power is illustrated in Figure 1 (b), where $I_{sp} = T/(qg_0)$.

As is shown in the previous graphs, each thruster works with a minimum input power of 7 kW and maximum input power of 13.95 kW. Three fully autonomous thrusters are considered for this mission. It is important to notice that the maximum value of specific impulse, namely the minimum propellant consumption, corresponds to the maximum input power. For this reason, in order to use the least amount of propellant, is fundamental to use the thrusters at maximum power for as long as possible.

The spacecraft has solar arrays that produce 47 kW of electric power at 1 AU (initial and final position of the mission), but 5 kW must be reserved for on board electronics. The array power is assumed to vary in an inverse relation with the squared distance from the Sun, and hence the available power for thrusting is $\mathrm{P_a}= 47/r^2 - 5$ kW, with r in AU. A 90% duty cycle is considered. Thrust magnitude and direction are the problem control variables. These propulsion assumptions are similar to those used in the development of the Asteroid Redirect Robotic Mission reference trajectory.

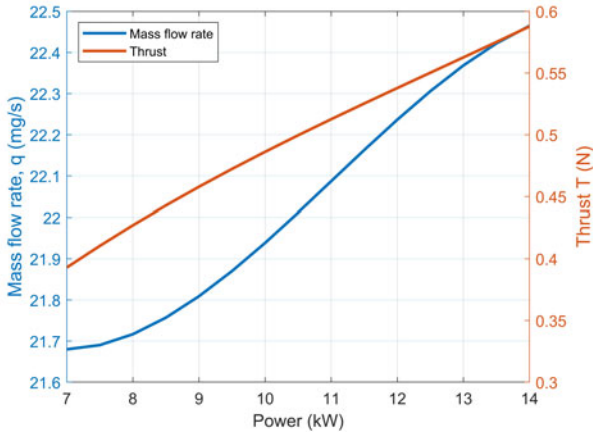

(a) Thrust and flow mass rate

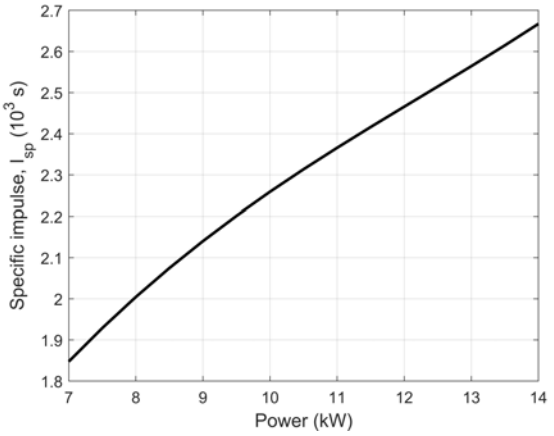

(b) Specific impulse

Figure 1. Thruster performance as a function of input power

3. Optimization of the segments

In order to find the optimal control law for the thrusters indirect methods are used. As said, these methods are based on the theory of optimal control [1] and solve the optimization problem by defining and solving a boundary value problem [2]. An adjoint variable is associated with each differential equation and

the Hamiltonian is defined. The usual expression is:

$$H = \boldsymbol{\lambda}_r^T \boldsymbol{v} + \boldsymbol{\lambda}_v^T \boldsymbol{g} + T S_F \tag{19}$$

where the thrust coefficient

$$S_F = \frac{\lambda_v^T \boldsymbol{T}/T}{m} - \lambda_m \frac{q}{T} \tag{20}$$

is named the *switching function*.
The theory of optimal control provides differential equations for the control and adjoint variables (Euler-Lagrange equations), and also boundary conditions for optimality, which depend on performance index and applied boundary conditions. The application of this theory produces a boundary value problem defined by the following properties:

- time interval for integration is divided into several sub-intervals where differential equations may have different expressions, and durations of each sub-interval are generally unknown;
- boundary conditions may be non-linear and must be satisfied at the relevant points;
- variables may be discontinuous and their values may be unknown after a discontinuity.

A multiple shooting technique is adopted to solve the resulting multipoint boundary value problem, which is transformed into a series of initial value problems leading to convergence by means of Newton's method [17]. In particular, error gradients are accurately evaluated and small corrections on the tentative solutions are done. More details regarding this numerical procedure are outlined in the work of F. Simeoni, L. Casalino et al. [18]. Differential equations of motion are integrated by using a variable-order variable-step integration scheme, based on the Adams-Moulton formulas [19], in order to carry out a fast and very accurate integration.
The optimal controls must maximize H at any given point along the trajectory, in agreement with PMP. One deduces that the thrust must be parallel to the velocity adjoint vector $\boldsymbol{\lambda}_v$ and the switching function becomes:

$$S_F = \frac{\lambda_v^T}{m} - \lambda_m \frac{q}{T} \tag{21}$$

If the propulsion system has constant effective exhaust velocity $c = T/q$, the thrust magnitude is the only remaining control, and one easily recognizes that a bang-bang control is required. The thrust assumes its maximum value when $S_F > 0$, whereas the engine is switched off when $S_F < 0$. Only in special cases, usually involving atmospheric flight, the switching function remains null along a non-zero interval and the thrust assumes an intermediate value (singular arc). PMP requires the maximization of S_F. In the general case of non-constant c the function

$$\bar{H} = T - q \frac{m \lambda_m}{\lambda_v} \tag{22}$$

must be maximized. It is interesting to note that $\bar{H}$ is a linear combination of T and q, and it depends on a single parameter $K = \frac{m\lambda_m}{\lambda_v}$, which is varying along the trajectory. At any given trajectory point, K is known and the power level that maximizes $\bar{H}$ must be sought. The problem is more complex when more than one engine is available and the electric power is split between the engines. Each thruster provides its own thrust and has its own propellant consumption, which both depend on its input power. $\bar{H}$ becomes:

$$\bar{H} = \sum_{i=1}^{N} T_i - K q_i \tag{23}$$

Three equal thrusters ($N = 3$) will be considered here. By introducing the coefficients $d_j = a_j - K b_j$, with $j = 0, 1, 2, 3$, one has:

$$\bar{H} = \sum_{i=1}^{3} d_0 + d_1 P_i + d_2 P_i^2 + d_3 P_i^3 = \sum_{i=1}^{3} f_i \tag{24}$$

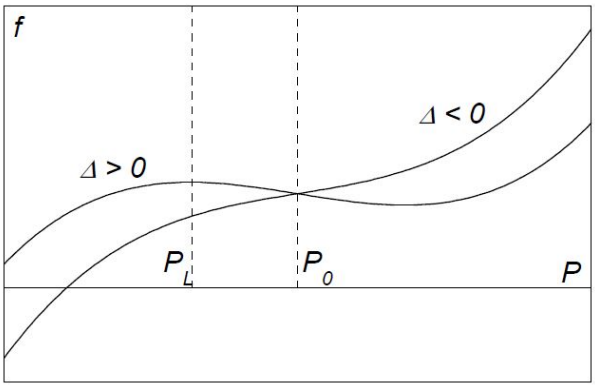

Figure 2. Generic behaviour of function f

The function $f = c_0 + c_1 P + c_2 P^2 + c_3 P^3$ is shown in Figure 3 with arbitrary scales for $c_3 > 0$, which is the case considered here. The curve second

derivative changes its sign from negative to positive at $P_0 = -c_2/(3c_3)$. Two cases exist, depending on $\Delta = c_2^2 - 3c_1c_3$, the discriminant of the quadratic equation that nullifies the first derivative of f. When $\Delta > 0$ a local maximum exists at $P = P_L = -P_0 - \sqrt{\Delta}/(6c_3)$, with a local minimum at a symmetric position with respect to P_0. The curve is stationary at P_0 for $\Delta = 0$. The curve is monotonic and no stationary points exist for $\Delta < 0$.

Each engine can either be turned off ($P_i = 0$) or operate between minimum and maximum limits ($P_m \leq P_i \leq P_M$). In addition, the total power cannot exceed the available power, that is, $\sum_{i=1}^{3} P_i \leq P_a$. The determination of the optimal power partitioning at any trajectory point is turned into finding P_1, P_2, P_3 that maximize $\bar{H}$, that is, a cubic function of the three variables, with the linear constraints $P_i = 0$ or $P_m \leq P_i \leq P_M$ and $\sum_{i=1}^{3} P_i \leq P_a$. Feasible solutions satisfy all the constraints. At a feasible point, a constraint is said to be active when the equality sign holds; it is said to be inactive when a strict inequality holds. Local maxima of $\bar{H}$ are sought for any combination of active and inactive constraints, and then compared to select the global maximum.

The function $\bar{H}$ is a locally maximum if its variation is non-positive for any admissible variation of the control variables. The constrained maximization problem is treated with an approach based on Lagrangian multipliers μ: Instead of $\bar{H}$, the augmented function:

$$\begin{aligned} \bar{H}^* = &\sum_{i=1}^{3} f_i + \mu_a\left(\sum_{i=1}^{3} P_i - P_a\right) + \\ &+ \mu_{i,M}\left(\sum_{i=1}^{3} P_i - P_M\right) + \mu_{i,m}\left(\sum_{i=1}^{3} P_i - P_m\right) \end{aligned} \tag{25}$$

is maximized.

More details of the optimal power partitioning are discussed in the paper of Casalino and Vavrina [20].

4. Results

Orbits of Eros and Earth are non-coplanar, with an angle of 10.82° between the two planes [16]. Therefore, on the Earth's orbit, there are two antipodal nodes in common with the plane of Eros: the one closer to the perihelion of Eros is temporally located around December, while the one closer to the aphelion of Eros is temporally located around June [16]. In order to have an initial orbital plane change without any propellant consumption, the departure from the Earth's Hill sphere is located arbitrarily in one of the two above-mentioned nodes of the Earth's orbit. This manoeuvre can be achieved with the escape velocity given by the launcher and possibly with Moon fly-bys. For the same reason, the Earth gravity assist of the inbound flight is located in the node closer to the perihelion of Eros, which is a much more convenient position for the fly-by than the other node, due to the eccentricity of the Eros' orbit.

Because of these geometric aspects of the problem, there are many different departure periods of the outbound journey. In fact, in a same year, the mission may start either in the period of December (node close to the aphelion of Eros), or in the period of June (node close to the perihelion of Eros). Nevertheless, a same departure from a specific node, but in different years, may have different performances in terms of optimal consumption, due to the synodic period between Earth and Eros, which is about 2.31 years [16]. In the same way, there are different periods of fly-by for the inbound journey. Hence, is possible to define a *family* of trajectories as a cluster of trajectories with the same period of departure or fly-by (depending if it is an outbound or an inbound one) and different durations.

Optimization results are presented separately for the outbound and inbound trajectory. Few explicative examples are chosen among all the found trajectories.

4.1. Outbound flight

Preliminary solutions of the outbound flight are found by removing the constraint of the asteroid rendezvous, imposing instead only the arrival in a generic point of Eros' orbit, not caring about the real presence of the asteroid. In this way, is possible to find an hypothetical trajectory with the best performance in terms of propellant consumption. From this ideal solution, the first families of the outbound journey are found adding back the rendezvous constraint. Other families are found in different periods by shifting the arrival and departure dates of these families. In Figure 3 are shown the arrival mass m_1 on Eros as a function of the flight duration for all the found families of the outbound journey. Obviously, the larger is the arrival mass the less is the propellant consumption. Depending on the family and duration, m_1 varies between 7000 Kg and 7900 Kg.

As one can see, to a longer duration of the flight corresponds a minor amount of requested propellant to arrive on Eros, since it is possible to manage more efficiently the thrust control as it will be further discussed. An other important aspect to notice is the different optimized arrival masses for a same duration: these differences are due to the phase of Earth and Eros, and the available electric power along the trajectory, which depends on the spacecraft's position relative to the Sun.

Two different outbound trajectories (projected in the ecliptic plane) with the same duration of about 4 years are compared in Figure 4, where departure and arrival

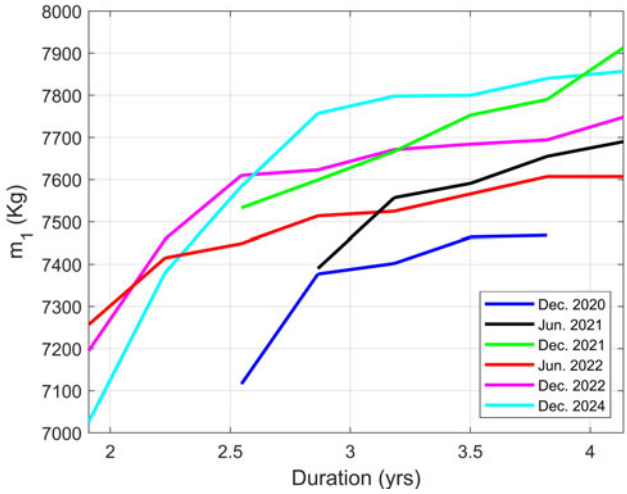

Figure 3. Arrival mass on Eros for the different families of the outbound journey

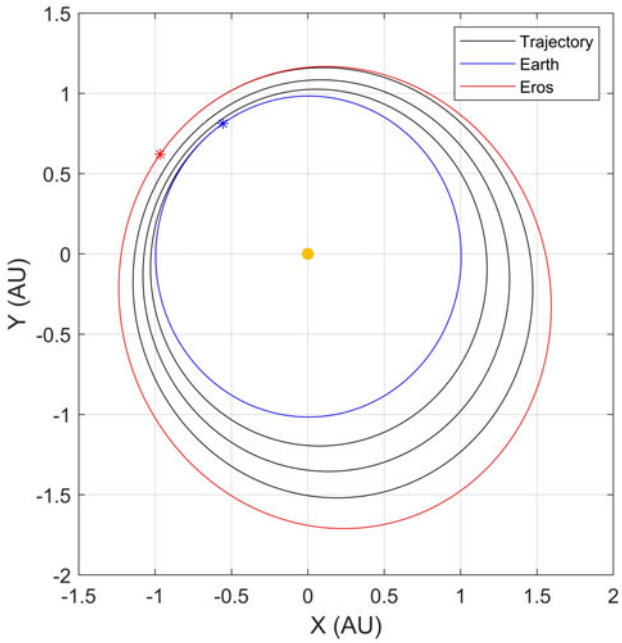

(a) Departure in December 2021

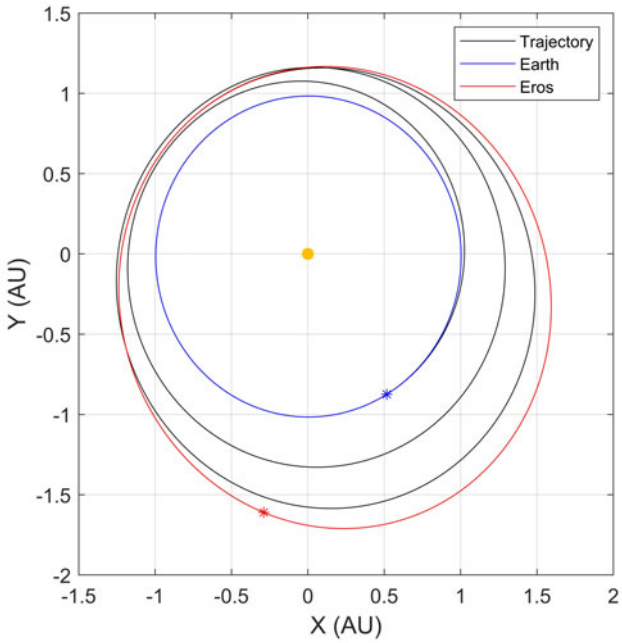

(b) Departure in June 2022

Figure 4. Comparison of two outbound trajectories with the same duration of about 4 years

epochs are marked with an asterisk on the respective orbit. The trajectory belonging to the December 2021 departure family has an optimized arrival mass about 300 Kg grater than the arrival mass of the other trajectory, which instead belongs to the June 2022 departure family.

This comparison suggests that to a minor amount of used propellant corresponds a more gradual approach of the spacecraft to the asteroid's orbit. This is due the orbit phases of trajectories: if phase is favourable, a gradual adjustment of both perihelion and aphelion altitude is possible, if, instead, phase is less favourable, with a quick adjustment of one of the two altitudes is possible to correct the angular velocity, but with a greater consumption of propellant. In fact, regarding the trajectory in Figure 4 (b), in order to adjust the early orbit phase, angular velocity is reduced by quickly increasing perihelion altitude and, subsequently, slowly correcting aphelion altitude. For this reason, in this second case a larger mass of propellant is needed.

As said, also the available electric power along a trajectory influences its performance in terms of propellant consumption. This aspect may be clearly visible comparing the control laws of the thrusters for the same two trajectories seen previously. This second comparison is presented in Figure 5.

The orange curve is the power P_a which is available for thrusting, and depends on the spacecraft's position relative to the Sun. The black, green and red curves are the electric power P_i used by each thruster, while the blue curve is the cumulative power P_T used by all the three thrusters. As shown in the graphs, in both cases the number of switched on thrusters depends on the amount of available electric power, and, where it is possible, the working power of each of them is equal to the maximum value of about 14 kW. In order to

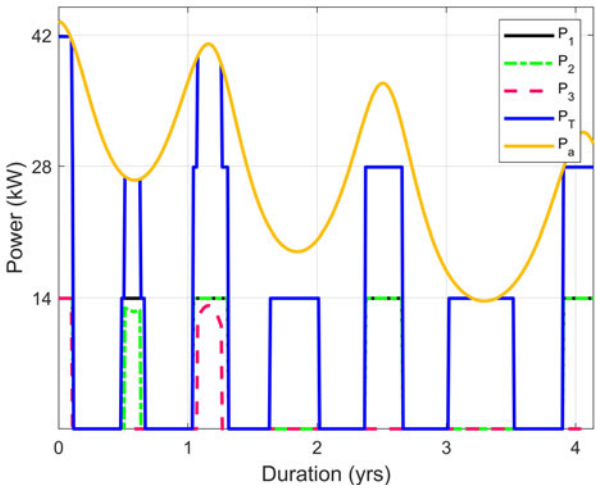

(a) Departure in December 2021

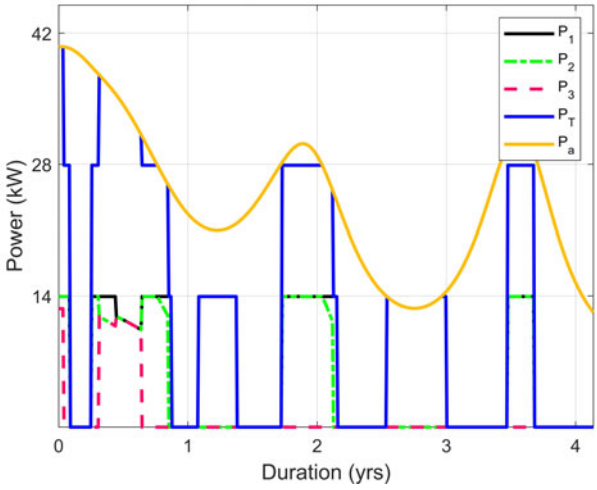

(b) Departure in June 2022

Figure 5. Comparison of the control laws for the same previous trajectories

better figure out how many engines are switched on, on the y-axis are highlighted the multiple values of the maximum power of each thruster (i.e. about 14 kW). The trajectory in Figure 5 (b) has a cumulative electric energy minor than the other trajectory, since this latter has more and higher peaks of available power. Therefore, in the first case, to use thrusters at maximum power (that is, maximum specific impulse) is easier, and a less amount of propellant is needed.
In Figure 6 the thrust vectors along the December 2021 departure 2D trajectory are shown. From this visualization is clear once again that the number of switched on engines depends on the spacecraft's position relative to the Sun. For this reason, the thrust segment with the greatest intensity of thrust vectors (about 1÷1.5 N) are placed in the most efficient positions in terms of available power, namely in proximity of the perihelion of the outbound trajectory. Is also possible to notice how thrust vectors in this case (and in almost every outbound trajectory) are substantially tangential to the trajectory.

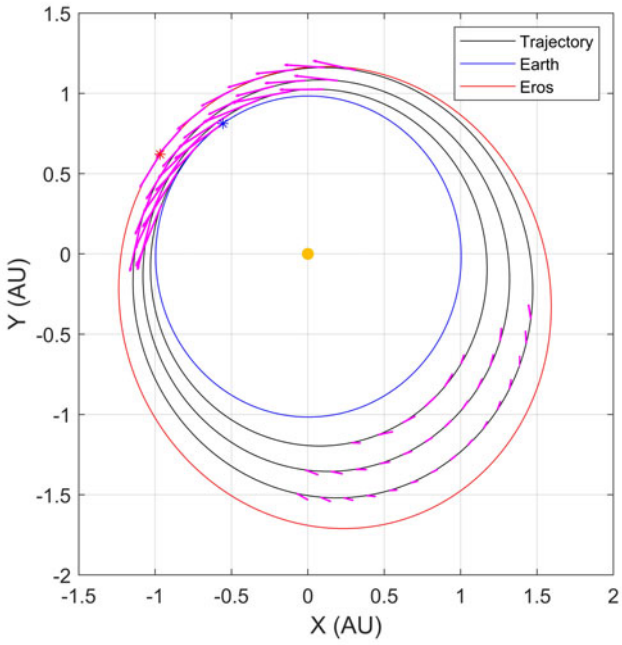

Figure 6. Thrust vectors along the December 2021 departure trajectory

By analysing Figures 7 and 8 is possible to understand how the inclination of the trajectory varies along the journey. The angle ϕ is the angle between the position vector of the spacecraft and the ecliptic plane, where a reference frame centred in the Sun is used. As one can see, inclination varies only when trajectory passes for one of the nodes, and it remains unchanged between the passages. This is clearly visible also in the 3D vision of the trajectory, where the Z scale is enlarged to highlight the inclination of Eros' orbit.

4.2. Inbound flight

A similar analysis can be made for the inbound flight. In this case the optimization index to be maximized is the initial mass m_2 departing from Eros (which corresponds to the mass of grabbed boulder, having m_1 fixed), while the selected propellant mass to use for this flight is 2000 Kg.
As said, the inbound families ar characterized by the period of fly-by. Choosing a proper period of time,

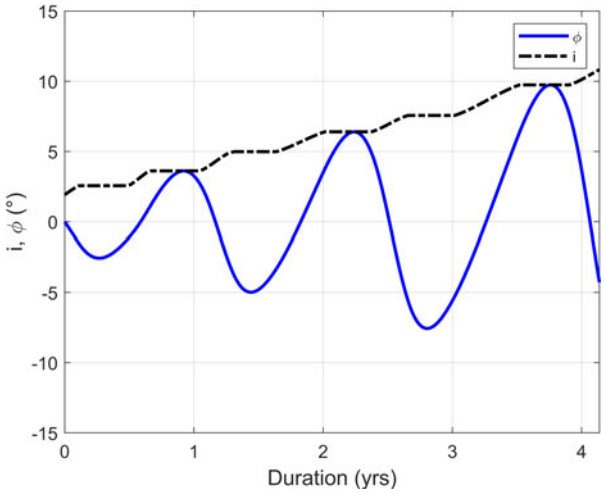

Figure 7. ϕ angle and inclination of the December 2021 departure trajectory

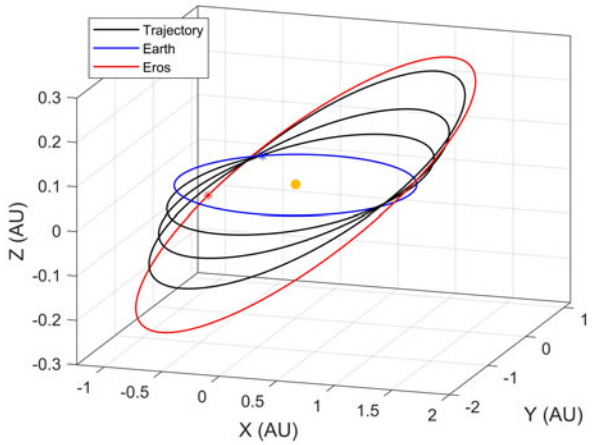

Figure 8. 3D vision of the December 2021 departure trajectory

in base of the arrival dates of the outbound trajectories, two families for the inbound journey are found, which both have fly-by in January 2028 and a similar value of the initial mass (m_2 is about 11000 Kg). By temporally shifting these two reference families of about 2 years back and forward, other two families are obtained with fly-by in January 2026 and 2030, respectively. Another family is found by temporally extending approximately by 6 months the Earth-Earth segment of the reference families (the ones with fly-by in January 2028). The best results in terms of initial mass are found in the early family with fly-by in January 2026 (m_2 is about 13900 Kg), while the worst results are found in the delayed family with fly-by in January 2030 (m_2 is about 8900 Kg). Evidently, due to the synodic periods of the bodies, the early family has the most efficient phase, while the other families are more distant from this optimal condition. The family with the extended Earth-Earth segment has an optimized initial mass slightly worse than the reference families (m_2 is about 10700 Kg). The above-mentioned geometric aspects, together with the available electric power, are again critical for a positive or negative performance in terms of optimized mass. More in detail, since the amount of propellant for the inbound journey is the same for every trajectory, the key for a better result is how efficiently it is possible to manage this amount of propellant in the Eros-Earth segment, in order to have a greater mass of propellant left to assist the fly-by in breaking the spacecraft and changing the plane towards the ecliptic plane. As for the outbound results, few explicative examples of the found trajectories are presented.

Two different inbound trajectories with the same duration of about 4 years are compared in Figure 9. The trajectory belonging to the January 2026 fly-by family has an optimized initial mass about 4900 Kg grater than the initial mass of the other trajectory, which instead belongs to the January 2030 fly-by family. Even in this case, departure and arrival epochs are marked with an asterisk on the respective orbit.

The Eros-Earth segment of the first trajectory in Figure 9 (a) is rather close to the Eros' orbit, while the same segment of the second trajectory has an aphelion much higher than the Eros' one. Therefore, in this second case, more propellant is needed to approach the Earth for a gravity assist. This difference in shape of the two trajectories is explicable looking at the control law graphs of the same two trajectories, which are shown in Figure 10. The fly-by epoch is pointed out on the x-axis.

The first and low peak of power in both figures coincides with the first passage of the spacecraft near the perihelion of Eros, as is possible to see in Figure 9. However, since the different departure epochs of these two cases, in the first trajectory the first peak is delayed of few months than the other one, so, in this way, is possible to use the low amount of power in the first year of journey to decrease perihelion of the orbit. Furthermore, in this first case, the control law avoid to use the first peak of power (using instead the phases of lower power near the aphelion), since, by switching on the thrusters in that position, the aphelion altitude would eventually increase too much, making necessary a greater amount of propellant to approach the Earth's orbit for gravity assist. This instead happens in the second case, where, because of the departure epoch, the control law is forced to use completely that peak of power at perihelion of the orbit in order to adjust

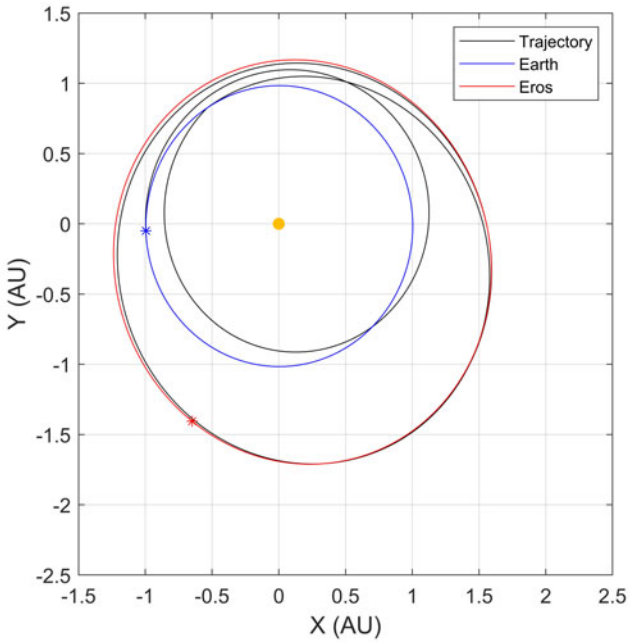

(a) Fly-by in January 2026

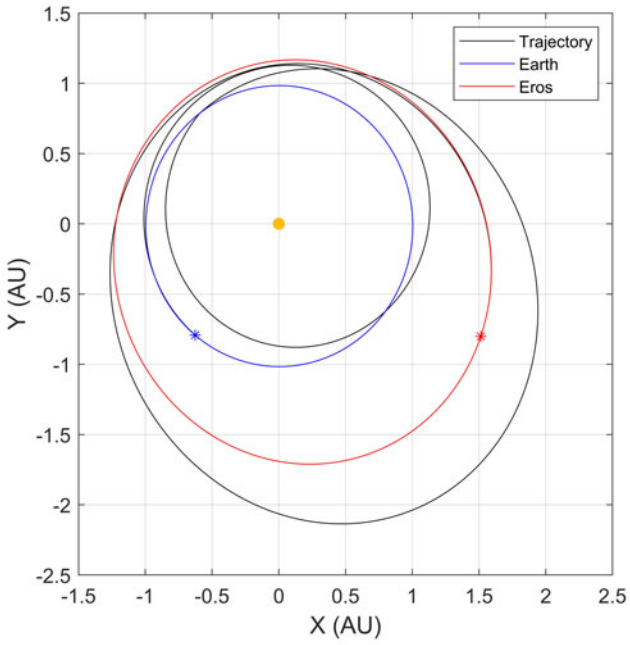

(b) Fly-by in January 2030

Figure 9. Comparison of two inbound trajectories with the same duration of about 4 years

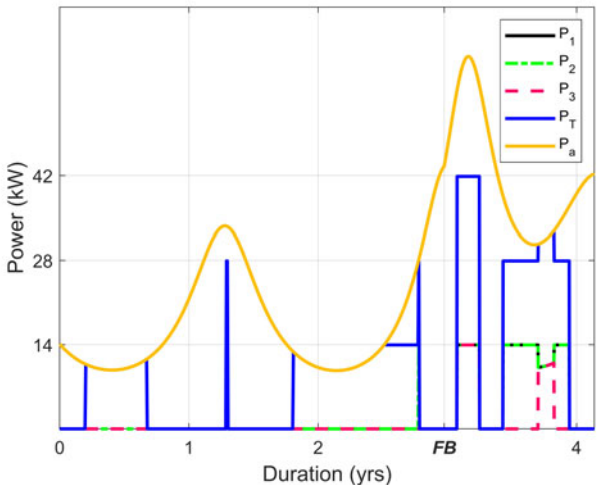

(a) Fly-by in January 2026

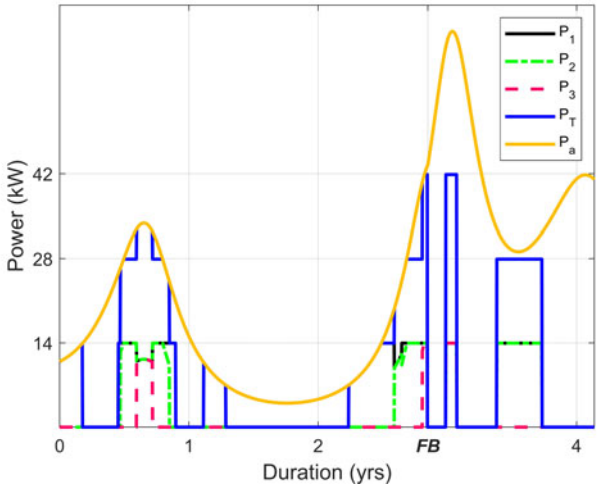

(b) Fly-by in January 2030

Figure 10. Comparison of the control laws for the same previous trajectories

the orbit phase.
In Figure 11 the thrust vectors along the January 2026 fly-by 2D trajectory are shown. This visualization confirms, as shown in Figure 10 (a), that in this case almost all of the propellant is used to break the spacecraft after the Earth fly-by. Unlike the trajectory in Figure 6, in this case (and in almost every inbound trajectory) thrust vectors have a significant radial component and are mostly not tangential to the trajectory. In the graph of ϕ and inclination of one of the previous trajectories is possible to see how almost all the inclination variation is due to the Earth fly-by. This is also clearly visible in the 3D vision of the trajectory, where again the Z scale is enlarged. These graphs are shown in Figure 12 and 13.

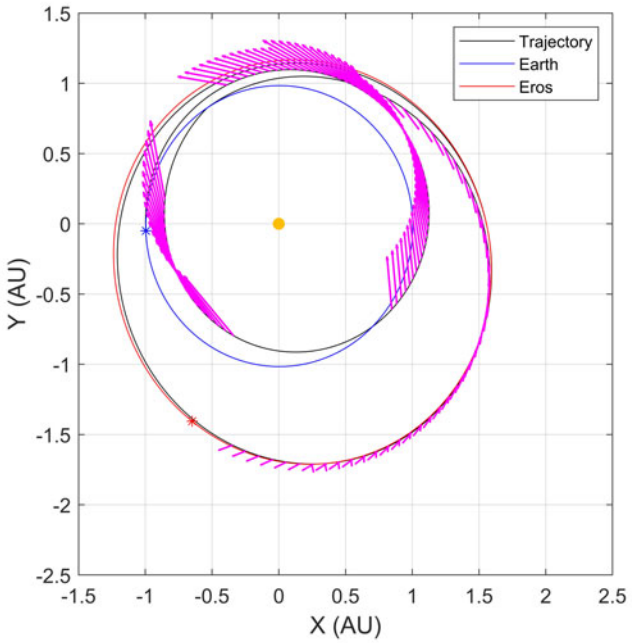

Figure 11. Thrust vectors along the January 2026 fly-by trajectory

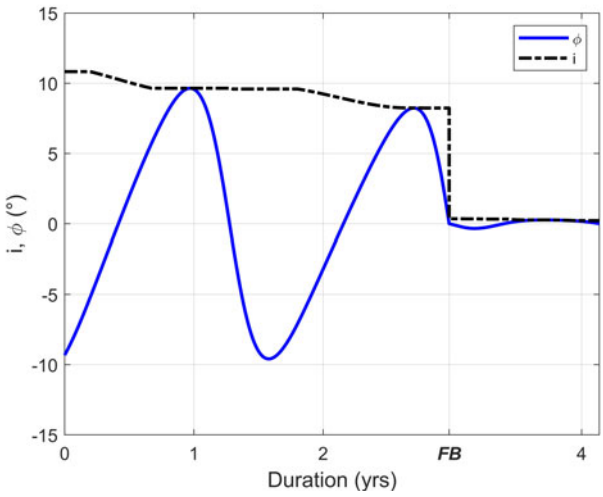

Figure 12. ϕ angle and inclination of the January 2026 fly-by trajectory

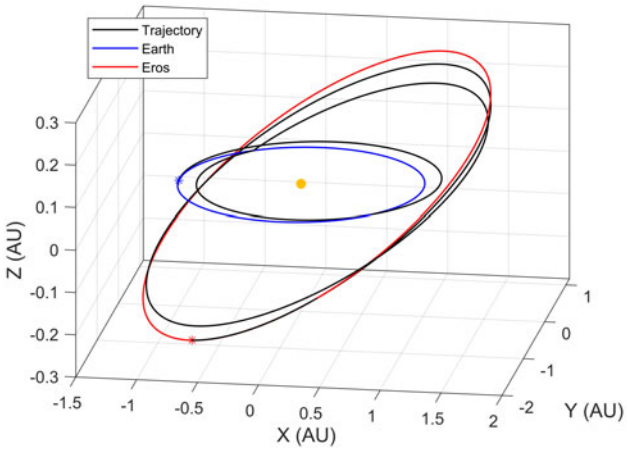

Figure 13. 3D vision of the January 2026 fly-by trajectory

5. Proposed missions

After all the possible trajectories for the outbound and inbound journey are collected, these are compared with each other in order to identify a final solution for this discussed mission. Then, two journeys are assembled if they respect two constraints: the minimum time interval on Eros must be of 6 months, in order to complete all the planned operations on the asteroid, and the mass of grabbed boulder must be at least of 2000 Kg, in order to satisfy the scientific requirements of the mission (the experiment of gravity tractor planned for the ARM [9]). Furthermore, as said, a second optimization of the inbound flight is done using the real amount of propellant left from the selected outbound flight.

Three different missions are proposed with mass of the boulder which respectively equals to: 4040 Kg, 5889 Kg, and 7014 Kg. The last one is the mission with the maximum mass of boulder transportable among all the possible combinations. Nevertheless, such a high mass may involve issues in terms of structures design and production costs. In this sense, the first two solutions may be preferable for a final choice. These first three solutions are presented in Tables 3-4. Finally, another solution for the mission is proposed using an initial mass of propellant of 4000 Kg, instead of 5000 Kg, and selecting the mission with the maximum mass of boulder. This analysis is carried out to test performance of the mission in case of a smaller initial mass of the spacecraft is needed. With this new condition the maximum mass of boulder found is 2138 Kg, slightly over the minimum mass. This result is shown in Table 5.

6. Conclusions

The cancelled NASA's Asteroid Redirect Mission [7] has been selected for a validation analysis of the opportune trajectories for a sample-return mission. Main

Table 2
1st proposed mission

Departure date from Earth	22 January 2022
Arrival and departure from Eros	4 April 2025 - 13 January 2026 (8 months)
Earth fly-by	26 January 2028
Arrival date on Earth	19 April 2029
Mass of the boulder	5889 Kg
Duration of mission	7 years and 5 months

Table 3
2nd proposed mission

Departure date from Earth	22 January 2022
Arrival and departure from Eros	16 March 2026 - 22 March 2027 (1 year)
Earth fly-by	26 January 2028
Arrival date on Earth	18 April 2029
Mass of the boulder	4040 Kg
Duration of mission	7 years and 5 months

Table 4
3rd proposed mission

Departure date from Earth	23 January 2021
Arrival and departure from Eros	3 July 2023 - 19 January 2024 (6 months)
Earth fly-by	26 January 2026
Arrival date on Earth	26 March 2027
Mass of the boulder	7014 Kg
Duration of mission	6 years and 4 months

purpose of the mission was to transfer a boulder from the surface of a NEA to a stable lunar orbit, where it could be further analysed by other missions. For this analysis the NEA (433) Eros has been selected. In order to quantify the mass of the transportable boulder inside the Earth's Hill sphere an optimization process of the trajectory has been carried out studying separately the outbound and inbound flight, considering an Earth gravity assist in the inbound leg. Commonly adopted approximations have been used. All the found trajectories of these two flights have been compared in order to identify a final solution for the mission. Few solutions have been proposed varying either the mass of boulder or the mass of initial propellant.

Table 5
Proposed mission with 4000 Kg of propellant

Departure date from Earth	22 January 2022
Arrival and departure from Eros	15 March 2026 - 28 August 2027 (1 year and 5 months)
Earth fly-by	28 January 2030
Arrival date on Earth	17 Oct. 2031
Mass of the boulder	2138 Kg
Duration of mission	9 years and 10 months

In the analysis conducted for the ARM the propellant used for the experiment of gravity tractor has not been taken into account. Since this experiment would last several weeks, the amount of propellant for this purpose may be significantly large. The amounts of propellant for orbit control around the asteroid and for ascending and descending manoeuvres are not considered as well. All these propellant contributions may vary critically the mass of boulder that the spacecraft can transport towards Earth, so, for this reason, a new and more accurate analysis of the mission could be necessary.

Another possible future analysis can be carried out by optimizing the trajectory in its entirety, instead of dividing it in two segments. In this way, better solutions may be obtained. Furthermore, optimization of the inbound flight can be performed again varying the final constraints at the entrance of the Earth's Hill sphere, in order to study the trajectory to the stable lunar orbit as well.

REFERENCES

1. A. E. Bryson and Y. C. Ho, *Applied Optimal Control: Optimization, Estimation, and Control*, New York, NY: Hemisphere, 1975. Revised printing.
2. L. Casalino, G. Colasurdo and D. Pastrone, "Optimal Low-Thrust Escape Trajectories Using Gravity Assist", *Journal of Guidance, Control, and Dynamics*, Vol. 22, No. 5 , pp. 637–642, 1999. https://arc.aiaa.org/doi/10.2514/2.4451
3. J. Veverka, M. Belton, K. Klaasen and C. Chapman, "Galileo's Encounter with 951 Gaspra: Overview", *Icarus*, Vol. 107, Is. 1, pp. 2–17, 2002. https://doi.org/10.1006/icar.1994.1002
4. L. A. D'Amario, L. E. Bright and A. Wolf, "Galileo trajectory design", *Space Science Reviews*, Vol. 60,

Is. 1-4, pp. 23–78, 1992. https://doi.org/10.1007/BF00216849
5. H. U .Auster, I. Richter, K. H. Glassmeier, G. Berghofer, C. M. Carr and U. Motschmann, "Magnetic field investigations during ROSETTA's 2867 Šteins fly-by", *Planetary and Space Science*, Vol. 58, Is. 9, pp. 1124–1128, 2010. https://doi.org/10.1016/j.pss.2010.01.006
6. H. Sierks, P. Lamy, C. Barbieri et al., "Images of Asteroid 21 Lutetia: A Remnant Planetesimal from the Early Solar System", *Science*, Vol. 334, Is. 6055 , pp. 487–490, 2011. http://science.sciencemag.org/content/334/6055/487
7. M. Gates, D. Mazanek, B. Muirhead, S. Stich, B. Naasz, P. Chodas, M. McDonald and J. Reuter, "NASA's Asteroid Redirect Mission Concept Development Summary", 2015 IEEE Aerospace Conference, Big Sky, Montana, USA, 2015. https://ieeexplore.ieee.org/document/7119163/
8. N. Strange, D. Landau, T. McElrath et al., M. McDonald and J. Reuter, "Overview of Mission Design for NASA Asteroid Redirect Robotic Mission Concept", 33rd International Electric Propulsion Conference (IEPC2013), Washington, D.C., 2013. http://hdl.handle.net/2014/44361
9. "NASA Announces Next Steps on Journey to Mars: Progress on Asteroid Initiative", NASA, 25 March 2015. https://www.nasa.gov/press/2015/march/nasa-announces-next-steps-on-journey-to-mars-progress-on-asteroid-initiative
10. D. D. Mazanek, J. Brophy and R. G. Merrill, "Asteroid Retrieval Mission Concept - Trailblazing Our Future in Space and Helping to Protect Us from Earth Impactors", Planetary Defense Conference, IAA-PDC13-04-14, 2013. https://ntrs.nasa.gov/archive/nasa/casi.ntrs.nasa.gov/20130013170.pdf
11. J. Brophy, F. Culick, L. Friedman et al., "Asteroid Retrieval Feasibility Study", Keck Institute for Space Studies, California Institute of Technology, Jet Propulsion Laboratory, Table 1: Asteroid Mass Scaling (for spherical asteroids), pp. 17, 2012. http://kiss.caltech.edu/final_reports/Asteroid_final_report.pdf
12. R. G. Merrill, M. Qu, M. A. Vavrina, C. A. Jones, and J. Englander "Interplanetary Trajectory Design for the Asteroid Robotic Redirect Mission Alternate Approach Trade Study", AIAA/AAS Astrodynamics Specialist Conference, AIAA SPACE Forum, San Diego, CA, USA, 2014 https://doi.org/10.2514/6.2014-4457
13. D. Landau, J. Dankanich, N. Strange et al., "Trajectories to nab a NEA (Near-Earth Asteroid)", AAS/AIAA Spaceflight Mechanics Meeting, Kauai, Hawaii, USA, 2013. http://resolver.caltech.edu/CaltechAUTHORS:20160223-161720457
14. J. Brophy, R. Gershman, D. Landau et al. "Asteroid Return Mission Feasibility Study", 47th AIAA/ASME/SAE/ASEE Joint Propulsion Conference & Exhibit, San Diego, California, USA, 2011. https://doi.org/10.2514/6.2011-5665
15. M. L. McGuire, N. J. Strange, L. M. Burke, S. L. McCarty, G. B. Lantoine, M. Qu, H. Shen, D. A. Smith and M. A. Vavrina, "Overview of the Mission Design Reference Trajectory for NASAs Asteroid Redirect Robotic Mission (ARRM)", AAS/AIAA Astrodynamics Specialist Conference, Stevenson, WA, USA, 2017. https://ntrs.nasa.gov/search.jsp?R=20170010282
16. 433 Eros (1898 DQ), JPL Small-Body Database Browser, 13 September 2009 (last observation). https://ssd.jpl.nasa.gov/sbdb.cgi?sstr=433
17. L. Casalino, G. Colasurdo and D. Pastrone, "Indirect optimization methodfor impulsive transfer", Astrodynamics Conference, Scottsdale, Arizona, USA, 1994. https://doi.org/10.2514/6.1994-3762
18. F. Simeoni, L. Casalino, A. Zavoli and G. Colasurdo, "Indirect Optimization of Satellite Deployment into a Highly Elliptic Orbit", International Journal of Aerospace Engineering, Vol. 2012, 2011. http://dx.doi.org/10.1155/2012/152683
19. L. F. Shampine and M. K. Gordon, *Computer Solution of Ordinary Differential Equations: The Initial Value Problem*, 1st ed., W.H. Freeman, San Francisco, CA, USA, 1975.
20. L. Casalino and M. A. Vavrina, "Optimal power partitioning for electric thrusters", AAS/AIAA Astrodynamics Specialist Conference, Stevenson, WA, USA, 2017. http://hdl.handle.net/11583/2680203